

# On the Automatic Parameter Selection for Permutation Entropy

A. Audun Myers<sup>1</sup> and Firas A. Khasawneh<sup>1</sup>*Department of Mechanical Engineering, Michigan State University, East Lansing, Michigan, 48824, United States of America.<sup>a)</sup>*

(Dated: 14 May 2022)

Permutation Entropy (PE) is a useful tool for time series analysis with a low computational cost. It has been used in many applications including damage detection, disease forecasting, detection of dynamical changes, and financial volatility analysis. However, to successfully use PE, an accurate selection of two parameters is needed: the permutation dimension  $n$  and embedding delay  $\tau$ . These parameters are often suggested by experts based on a heuristic or by a trial and error approach. Both of these methods can be time-consuming and lead to inaccurate results. We investigate multiple schemes for automatically selecting these parameters with only the corresponding time series as the input to help combat this issue. Specifically, we develop a frequency-domain approach based on the least median of squares and the Fourier spectrum, as well as extend two existing methods: Permutation Auto-Mutual Information Function (PAMI) and Multi-scale Permutation Entropy (MPE) for determining  $\tau$ . We then compare our methods as well as current methods in the literature for obtaining both  $\tau$  and  $n$  against expert-suggested values in published works. We show that the success of any method in automatically generating the correct PE parameters depends on the category of the studied system. Specifically, for the delay parameter  $\tau$ , we show that our frequency approach provides accurate suggestions for periodic systems, nonlinear difference equations, and ECG/EEG data, while the mutual information function computed using adaptive partitions provides the most accurate results for chaotic differential equations. For the permutation dimension  $n$ , both False Nearest Neighbors and MPE provide accurate values for  $n$  for most of the systems with a value of  $n = 5$  being suitable in most cases.

**Permutation Entropy (PE) is one of the simple yet very effective tools for studying time series of dynamical systems. It provides an information statistic that measures the complexity of a time series through the probability of unique ordinal patterns found within the time series called permutations. These permutations are symbolic representations obtained by encoding consecutive subsets of the data of a certain length using their ordinal ranking. However, the success of PE depends on the selection of both the spacing (delay  $\tau$ ) and size (dimension  $n$ ) of these permutations. Despite the wide use of PE, it is often unclear how these parameters must be selected with the most common approach relying on trial and error. This can lead to inaccurate results, and it can prevent applying PE to large data sets in the absence of automatic parameter selection algorithms. In this work we investigate various methods for automatically selecting both  $\tau$  and  $n$ . In addition to developing novel methods that facilitate the parameter selection, we also assess the accuracy of using classical time series tools for identifying permutation entropy parameters. The success of each of the investigated methods in computing  $\tau$  and  $n$  is determined based on a comparison with the corresponding values suggested by domain experts.**

information-based system. Information entropy was first introduced by Shannon<sup>46</sup> in 1948 as Shannon Entropy. Specifically, Shannon entropy measures the uncertainty in future data given the probability distribution of the data types in the original, finite dataset. Shannon entropy is calculated as  $H_s(n) = -\sum p(x_i) \log p(x_i)$ , where  $x_i$  represents a data type, and  $p(x_i)$  is the probability of that data type. In recent years information entropy has been heavily applied to the time series of dynamic systems. Several new variations of information entropy have been proposed to better accommodate these applications, e.g. approximate entropy<sup>39</sup>, sample entropy<sup>43</sup>, and PE<sup>4</sup>. These methods measure the predictability of a sequence through the entropy of the relative data types. However, PE considers the ordinal position of the data (permutations), which have been shown to be effective for analyzing the dynamic state and complexity of a time series<sup>1,5,11,18,21,22,33,36</sup>. PE is also noise robust for time series of sufficient length and relatively high signal-to-noise ratios, which is the ratio between useful signal and background noise. Alternatively, if the time series is relatively short and has a low signal-to-noise ratio, it is suggested to use a different entropy measurement such as coarse-grained entropies<sup>41</sup>. PE is quantified in a similar fashion to Shannon entropy with only a change in the data type to permutations (see Fig. 2), which we symbolically represent as  $\pi_i$ . PE has two parameters: the permutation dimension  $n$  and embedding delay  $\tau$ , which are used when selecting the permutation size and spacing, respectively. PE is sensitive to these parameters<sup>30,44,47</sup> and there is no accurate selecting approach. This introduces the motivation for this paper: investigate automatic methods for selecting both PE parameters. There are currently three main methods for selecting PE parameters: (1) use parameters suggested by experts for a specific application, (2) use trial and error to find suitable parameters, or (3) use methods developed for phase space reconstruction. We will now overview a simple example

## I. INTRODUCTION

Permutation Entropy (PE) has its origins in information entropy, which is a tool to quantify the uncertainty in an

<sup>a)</sup>Electronic mail: myersau3@msu.edu

to better understand these parameters.

Bandt and Pompe<sup>4</sup> defined PE according to

$$H(n) = -\sum p(\pi_i) \log p(\pi_i), \quad (1)$$

where  $p(\pi_i)$  is the probability of a permutation  $\pi_i$  and  $H(n)$  is the permutation entropy for dimension  $n$  with units of bits when the logarithm is of base 2. The permutation entropy parameters  $\tau$  and  $n$  are used when selecting the motif size, with  $\tau$  determining the time difference between two consecutive points in a uniformly sub-sampled time series and  $n$  as the permutation length or motif dimension. To form a permutation begin with an element  $x_i$  of the series  $X$ . Using this element, the dimension  $n$ , and delay  $\tau$ , define the vector  $v_i = [x_i, x_{i+\tau}, x_{i+2\tau}, \dots, x_{i+(n-1)\tau}]$ . The corresponding permutation  $\pi_i$  of this vector is determined using its ordinal pattern. For example, consider the third degree  $n = 3$  permutation shown in Fig. 1. The permutation type, which categorizes

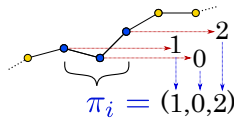


FIG. 1. Sample permutation formation for  $n = 3$  and  $\tau = 1$ .

the permutation, is found by first ordering the  $n$  values of the permutation smallest to largest, and then accounting for the order received. For the given permutation in Fig. 1, the resulting permutation is categorized as the sequence  $\pi_i = (1, 0, 2)$ , which is one of  $n!$  possible permutations for a dimension  $n$ , see Fig. 2.

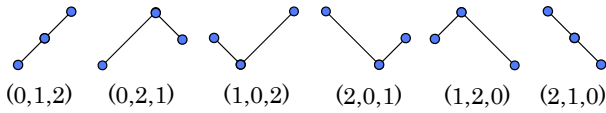


FIG. 2. All possible permutation Configurations for  $n = 3$ .

We can normalize PE using the maximum possible PE value, which occurs when all  $n!$  possible permutations are equiprobable according to  $p(\pi_1) = p(\pi_2) = \dots = p(\pi_{n!}) = \frac{1}{n!}$ . The resulting normalized PE is

$$h_n = -\frac{1}{\log_2 n!} \sum p(\pi_i) \log_2 p(\pi_i). \quad (2)$$

A toy example demonstrating the calculation of  $h_n$  is provided in the appendix.

Many domain scientists who apply PE make general suggestions for  $n$  and  $\tau$ <sup>19,52</sup>. Unfortunately, using these suggested parameters can result in unuseful calculations of PE. As an example of this shortcoming, Popov et al.<sup>40</sup> applied PE to electroencephalogram (EEG) data and showed that the sampling frequency influences the selection of  $\tau$ . As for the dimension  $n$ , there are only general suggestions on how to choose its value. For example, the appropriate permutation dimension lies in the range  $3 < n < 8$  for the vast majority of applications<sup>44</sup>. Additionally, Bandt and Pompe<sup>4</sup> suggest that  $N \gg n$ ,

where  $N$  is the length of the time series. However, these general outlines for the selection of  $n$  (and  $\tau$ ) do not allow for an application specific suggestion for  $n$ .

If we assume that suitable PE parameters correspond to optimal phase space reconstruction parameters, then a common approach for selecting  $\tau$  and  $n$  is to implement one of the existing methods for estimating the optimal Takens' embedding<sup>49</sup> parameters. Hence, some of the common methods for determining  $\tau$  include the mutual information function approach<sup>20</sup>, the first folding time of the autocorrelation function<sup>8,23</sup>, and phase space methods<sup>10</sup>. Additionally, some common phase space reconstruction methods for determining  $n$  include box-counting<sup>7</sup>, correlation exponent method<sup>23</sup>, and false nearest neighbors<sup>25</sup>. Although the parameters in PE have similar names to their delay reconstruction counterpart, there are innate differences between ordinal patterns and phase space reconstruction which can also lead to inaccurate  $n$  or  $\tau$  values. In spite of these differences, permutations can be viewed as symbolic representation of regions in the phase space through a binning process. Permutations partition the phase space based on the ordinal rankings of the embedded vectors. This relationship between phase space and permutations opens up the potential for some of the classic phase space reconstruction methods for selecting both  $n$  and  $\tau$  to be a plausible solution for selecting the same parameters for PE.

Even with the possibility that phase space reconstruction methods for selecting  $\tau$  and  $n$  may work for choosing synonymous parameters of PE, there are a few practical issues that preclude using parameters from time series reconstruction for PE. For example, many of the methods (e.g. false nearest neighbors and mutual information) still require some user input through either a parameter setting or user interpretation of the results. This introduces issues for practitioners working with numerous data sets, or those without enough expertise in the subject area to interpret the results. Another issue that arises in practice is that the algorithmic implementation of existing time series analysis tools is nontrivial. This hinders these tools from being autonomously applied to large datasets. For example, the first minimum of the MI function is often used to determine  $\tau$ . However in practice there are limitations to using mutual information to analyze data without the operator intervention to sift through the minima and choose the first 'prominent' one. Specifically, the mutual information function can have small kinks that can be erroneously picked up as the first minimum. Figure 3a shows this situation where the first minimum of the mutual information function for a periodic Lorenz system is actually an artifact, and that the actual delay should be at the local minimum with  $\tau = 11$ . Further, the mutual information function approach may also fail if the mutual information is monotonic. This is a possibility since there is no guarantee that minima exist for mutual information<sup>3</sup>. An example of this mode of failure is shown in Fig. 3b, which was generated using EEG data<sup>2</sup> from a patient during a seizure.

Another mode of failure for the autocorrelation method can occur when the time series is non-linear or has a moving average. In this case, the autocorrelation function may reach the folding time at an unreasonably large value for  $\tau$ . As an exam-

ple, Fig. 3c shows the autocorrelation not reaching the folding time of  $\rho = 1/e$  until a delay of  $\tau = 283$  for electrocardiogram data provided by the MIT-BIH Arrhythmia Database<sup>35</sup>. The last mode of failure concerns choosing the permutation dimension  $n$  to be equal to the embedding dimension optimized using delay embedding from time series analysis. This can lead to an overly large embedding dimension<sup>12</sup> ( $n \gg 8$ ), which would make the calculation of PE impractical because the number of possible permutations  $n!$  would become too large. All of these possible modes of failure can make using

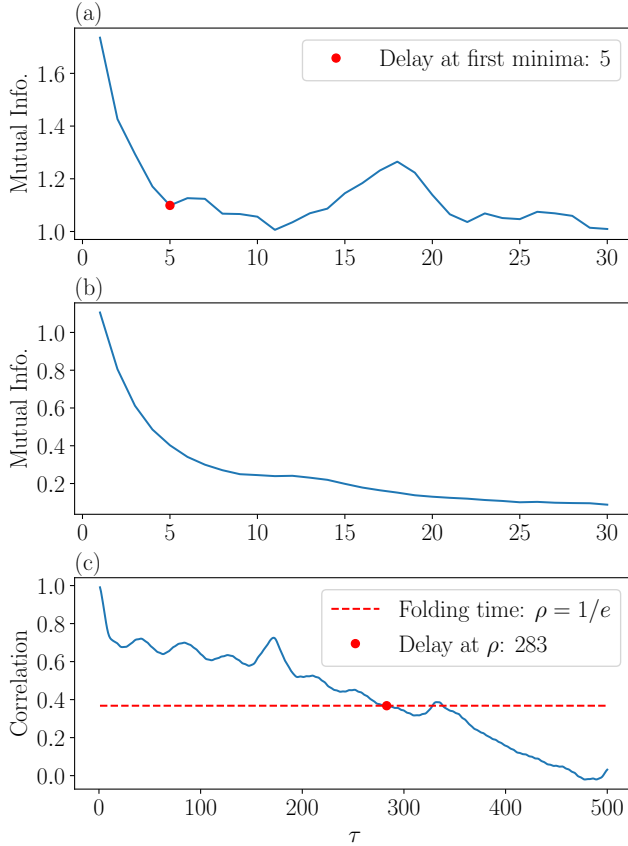


FIG. 3. Some possible modes for failure for selecting  $\tau$  for phase space reconstruction using classical methods: (a) mutual information registering false minima as suitable delay generated from a periodic Lorenz system, (b) mutual information being mostly monotonic and not having a distinct local minimum to determine  $\tau$  generated from EEG data<sup>2</sup>, and (c) autocorrelation failing from a moving average of ECG data provided by the MIT-BIH Arrhythmia Database<sup>35</sup>.

classical phase space methods for selecting  $\tau$  and  $n$  unreliable thus necessitating new tools or modifications to make selecting  $\tau$  and  $n$  for PE more robust and less user-dependent.

These shortcomings lead us to the problem we address in this paper: Given a sufficiently sampled/oversampled, noisy time series  $X = \{x_t\}_{\mathcal{R}^+}$ , how can we reliably and systematically define appropriate dimension  $n$  and time delay  $\tau$  values for computing the corresponding PE?

Our first contribution towards answering this question is detailed in Section II and it is related to the automatic selection

of the time delay  $\tau$ . Specifically, assuming that  $X$  is contaminated by Gaussian measurement noise, in Section II A we combine the Least Median of Squares (LMS) approach for outliers detection with Fourier transformation theorem to derive a formula for the maximum significant frequency in the Fourier spectrum. This formula allows obtaining a cutoff value where the only input, besides the time series, is a desired percentile from the Probability Density Function (PDF) of the Fourier spectrum. Once this value is obtained, Nyquist's sampling theorem is used to compute an appropriate  $\tau$  value.

The second contribution is through an approach that we develop in Section II B, which uses Multi-scale Permutation Entropy (MPE) for finding  $\tau$ . We show how MPE can be used to find the main period of oscillation for a time series derived from a periodic system. Building upon this, we show how the method can be extended to find  $\tau$  for a chaotic time series by using the first maxima in the MPE. Specifically, we suggest using the delay  $\tau$  at the first maxima for PE calculations as it satisfies the Nyquist's sampling theorem.

Our third contribution to the automatic selection of  $\tau$  is through the analysis of Permutation Auto-Mutual Information<sup>31</sup> (PAMI). PAMI is an existing method for measuring the mutual information of permutations. However, in this paper we tailor this method to specifically select  $\tau$  for PE.

Our final contribution towards answering the posited question is our evaluation of the ability of existing tools for computing an embedding dimension to provide an appropriate value for the PE parameter  $n$ . We compare  $n$  values computed from False Nearest Neighbors (FNN—Section III A), Singular Spectrum Analysis (SSA—Section III B), and MPE (Section II B). While we use existing methods for performing the FNN and the SSA analyses, for the MPE-based approach, we use a criteria established in prior works<sup>44</sup>, which requires finding  $\tau$  first, for selecting  $n$ . We made this process automatic through the selection of  $\tau$  from our second contribution.

This paper is organized as follows. We first go into detail on some existing methods for selecting both  $\tau$  and  $n$ . Specifically, in Section II we provide a detailed explanation for selecting  $\tau$  using existing, automatic methods such as autocorrelation in Section II C and Mutual Information (MI) in Section II D. Additionally, we modify and develop/tailor methods to automatically select  $\tau$ . These methods include a frequency approach in Section II A, MPE in Section II B, and PAMI in Section II E. In Section III we expand on the process for selecting  $n$  using False Nearest Neighbors (FNN) in Section III A and Singular Spectrum Analysis in Section III B. In Section III C, we explain our algorithm for automatically selecting  $n$  using MPE. After introducing each method, in Section IV we contrast all of these methods and make conclusions on their viability by comparing the resulting parameters to those suggested by PE experts. An overview of the methods that will be investigated for automatically calculating both  $\tau$  and  $n$  are shown in Fig. 4

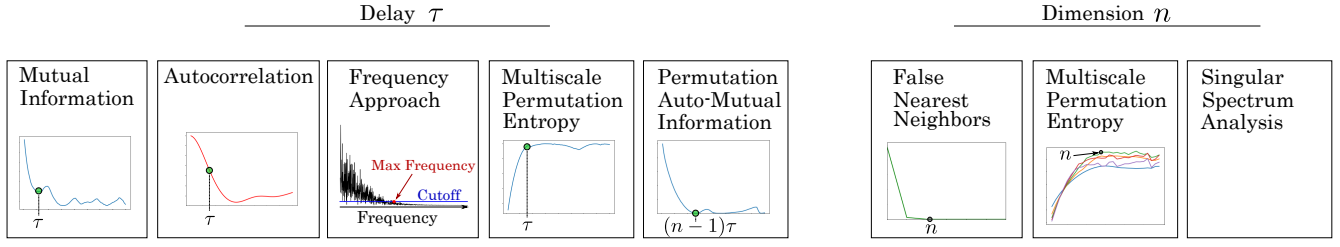


FIG. 4. Overview of methods investigated for automatically calculating both the delay  $\tau$  and dimension  $n$  for permutation entropy.

## II. METHODS FOR EMBEDDING DELAY PARAMETER SELECTION

The delay embedding parameter  $\tau$  is used to uniformly subsample the original time series. To elaborate, consider the time series  $X = \{x_i \mid i \in \mathbb{N}\}$ . By applying the delay  $\tau \in \mathbb{N}$ , a new subsampled series is defined as  $X(\tau) = [x_0, x_\tau, x_{2\tau}, \dots]$ . In order to obtain a stable and automatic method for estimating an optimal value for  $\tau$  we investigate: a novel frequency-based analysis that we describe in Section II A, Multi-scale Permutation Entropy (MPE) (Section II B), autocorrelation (Section II C), and Mutual Information function (MI) (Section II D). We recognize, but do not investigate, some other methods for finding  $\tau$  such as diffusion maps<sup>6</sup> and phase space expansion<sup>10</sup>.

### A. Frequency Approach for Embedding Delay

In this section, we develop a method for finding the noise floor in the Fourier spectrum using Least Median of Squares (LMS)<sup>32</sup>. We then use the noise floor to find the maximum significant frequency of a signal contaminated with additive Gaussian white noise (GWN). Our method is based on finding the maximum significant frequency in the Fourier spectrum and the Nyquist sampling frequency criteria. To motivate the development of this approach, we begin by working with the frequency criteria developed by Melosik and Marszalek<sup>34</sup>, which agrees with Nyquist sampling theorem<sup>27</sup>, for choosing a suitable sampling frequency  $f_s$ :

$$2f_{\max} < f_s < 4f_{\max}, \quad (3)$$

where  $f_{\max}$  is the maximum significant frequency in the signal. Melosik and Marszalek<sup>34</sup> showed that a sampling frequency within this range is appropriate for subsampling an oversampled signal, thus mitigating the effect of temporal correlations of neighboring points in densely sampled signals. However, the automatic identification of  $f_{\max}$  from an oversampled signal is not trivial. Melosik and Marszalek<sup>34</sup> selected a maximum significant frequency by inspecting the normalized Fourier spectrum and using a threshold cutoff of approximately 0.01 for a noise-free chaotic Lorenz system. This made *visually* finding the maximum frequency significantly easier but did not provide guidance on how to algorithmically find  $f_{\max}$ . Further, attempting to algorithmically adopt the approach suggested by Melosik and Marszalek<sup>34</sup> resulted

in large errors especially in the presence of a low signal to noise ratio. Therefore, this motivated the search for an automatic, data-driven approach for identifying the noise floor, which could then be used to find the maximum significant frequency. This led us to develop a method that is based on 1-D least median of squares applied to the Fourier spectrum, which we describe below. The assumptions inherent to our method are

1. The time series is not undersampled. The purpose of the methods is to determine a suitable delay parameter for subsampling the signal, which would be meaningless if the time series is undersampled.
2. The Fourier transform of the time series needs to have less than 50% of the points with significant amplitudes. This requirement stems from the limitations of the least median of squares regression.
3. The noise in the signal is approximately GWN; otherwise, the ensuing statistical analysis becomes inapplicable. Violating this assumption can yield false peak detections, which would lead to an incorrect delay parameter.

We find suitable cutoffs for obtaining  $f_{\max}$  of the signal by using the noise floor determined from the 1-D least median of squares, and compute a suitable embedding delay according to

$$\tau = \frac{f_s}{\alpha f_{\max}}, \quad (4)$$

where we set  $\alpha = 2$ , thus agreeing with the range in Eq. (3) and the Nyquist sampling criterion.

Figure 5 summarizes the frequency approach for  $\tau$  with the use of our 1-D LMS method for finding a noise floor in the Fourier spectrum. This process begins with computing the Fourier spectrum signal, which is followed by fitting an LMS regression line to the noise in the Fourier spectrum. This provides statistical information about the Probability Distribution Function (PDF) of the noise level. The PDF is used to determine the Cumulative Distribution Function (CDF), which can be used to determine a meaningful noise cutoff in the Fourier spectrum. However, if noise is present, it must be approximately GWN for this method to hold statistical significance. This cutoff is used to separate the highest significant frequency in the Fourier spectrum  $f_{\max}$ , which is used to find a suitable embedding delay  $\tau$  based on the frequency criteria in

Eq. (4). In the following paragraphs we review our use of the LMS and the derivation of the PDF of the Fourier spectrum of GWN. We then show how to combine the LMS method with the resulting PDF expression to find a suitable noise floor cutoff and the corresponding maximum significant frequency.

*a. Least Median of Squares:* LMS is a robust regression technique used when up to 50% of the data is corrupted by outliers. Outliers will be considered as anything other than noise in the fourier spectrum for our application. The algorithm for LMS regression was initially published in 1984 by Massart et al.<sup>32</sup>. In comparison to the widely used least sum of squares (LS) algorithm, the LMS replaces the sum for the median, which makes LMS resilient to outliers. The difference between LS and LMS can be described by

$$\begin{aligned} LS : \min \sum_i r_i^2, \\ LMS : \min (\text{median}_i(r_i^2)), \end{aligned} \quad (5)$$

where  $r$  is the residual. Similar to the  $i$  subscript in  $\sum_i$ , the  $i$  in  $\text{median}_i$  signifies that the median is of all residuals. Figure 6 shows an example application of the linear LMS regression. Specifically, this figure shows 110 data points drawn from the line  $y = x + 1$  with added GWN of zero mean and 0.1 standard deviation. The data is corrupted with 90 outliers centered around (3, 2) with a normal distribution of 1.0 along  $x$  and 0.6 along  $y$ . Figure 6 shows that the linear regression results closely match the actual trend line with the fitted line being  $y = 0.998x + 1.012$  in comparison to the actual  $y = x + 1$ . These results agree well with the ones found in<sup>32</sup>.

*b. PDF and CDF of the magnitude of the Fast Fourier Transform of GWN:* This section reviews the probability distribution function (PDF) and cumulative density function (CDF) for the Fourier Transform (FT) of GWN. Additionally, this section derives the location of the theoretical maximum of the PDF. The FT distribution of GWN<sup>42</sup> is described as

$$P_{|X|}(|X|) = \frac{2|X|}{E_w \sigma_x^2} e^{\frac{-|X|^2}{E_w \sigma_x^2}}, \quad (6)$$

where  $|X|$  is the magnitude of the FT of GWN,  $P_{|X|}$  is the probability density function of  $|X|$ ,  $\sigma_x$  is the standard deviation of the GWN, and  $E_w$  is the window energy or number of discrete transforms taken during the FT. By setting the first derivative of  $P_{|X|}$  with respect to  $|X|$  equal to zero, the theoretical maximum of the PDF is

$$|X|_{\max} = \sqrt{\frac{E_w \sigma_x^2}{2}}. \quad (7)$$

We calculate the CDF corresponding to the PDF described in Eq. (7) by combining the PDF in Eq. (6) with the CDF for a Rayleigh distribution as<sup>37</sup>

$$CP_{|X|}(|X|) = 1 - e^{\frac{-|X|^2}{E_w \sigma_x^2}}, \quad (8)$$

where  $CP_{|X|}$  is the cumulative probability of  $|X|$ .

*c. Finding the Noise Floor:* Our approach for finding the noise floor combines LMS with Eqs. (6) and (7). Specifically, we utilize LMS to obtain a 1-D fit of the Fast Fourier Transform (FFT) of the signal, which results in an approximate value of  $|X|_{\max}$ , which is  $|X|$  at the maximum of  $P_{|X|}$ . Using  $|X|_{\max}$  from the LMS fit, we then find the standard deviation of the distribution  $\sigma_x$  from Eq. 7, which is used to find a cutoff based on a set cumulative probability in Eq. (8).

We begin by showing the accuracy of the LMS fit for finding  $|X|_{\max}$ . Our example uses GWN with a mean of zero and standard deviation of 0.035 with 1000 data points. Taking the FFT of the GWN (see Fig. 7A) results in the distribution shown in Fig. 7B. The distribution shows a 1-D LMS fit of 8.215 compared to the theoretical maximum of the PDF from Eq. 7 of 7.826, which is approximately 4.67% greater. This shows that the 1-D LMS fit accurately locates  $|X|_{\max}$ . Additionally, the theoretical shape of the PDF in Fig. 7B is shown to be very similar to the actual distribution.

Next, our approach utilizes Eq. (8) and  $\sigma_x$  derived from Eq. (7) for finding the cutoff value  $|X|_{\text{cutoff}}$ . The  $|X|_{\text{cutoff}}$  for a desired cumulative probability  $CP$  is found by solving Eq. (8) for  $|X|$  as

$$|X|_{\text{cutoff}} = \sqrt{-E_w \sigma_x^2 \ln(1 - CP)}. \quad (9)$$

In order to make  $|X|_{\text{cutoff}}$  robust to normalization and scaling of the FFT, we define the ratio  $C$  between the suggested cutoff from Eq. (9) and the maximum of the PDF from Eq. (7) as

$$C = \frac{|X|_{\text{cutoff}}}{|X|_{\max}} = \sqrt{-2 \ln(1 - CP)}. \quad (10)$$

*d. Example Cutoff:* An example of how Eqs. (7) and (9) are used is shown in Fig. 8, where the maximum of the PDF and the cutoff for  $CP = 99\%$  are marked in Fig. 8a and 8b, respectively. For this example, we find the ratio  $C$  to be approximately 3.03 for a 99% probability. In addition, we suggest a cutoff ratio  $C = 6$  to be used for signals with less than  $10^4$  data points. This yields an expected probability of  $\approx 10^{-8}\%$  for a point in the FFT of the GWN attaining a magnitude greater than  $|X|_{\text{cutoff}}$ . Alternatively, Eq. (10) can be used to calculate a different value of  $C$  based on the desired probability and length of the signal.

## B. Multi-scale Permutation Entropy for Selecting Delay

In this section, we develop a method based on Multi-scale Permutation Entropy (MPE) to find the periodicity of a signal, which is then used to find a suitable delay parameter. MPE is a method of applying permutation entropy over a range of delays, which was first introduced by Costa et al.<sup>14</sup> for analyzing physiological time series. Zunino et al.<sup>53</sup> showed how the first maxima in the MPE plot arises when  $\tau$  matches the characteristic time delay  $\tau_r$ . Furthermore, the periodicity can be captured by the first dip in the MPE plot as shown in Fig. 9 at the location  $d_2$  when the delay  $\tau$  matches the characteristic time delay  $\tau_r$ .



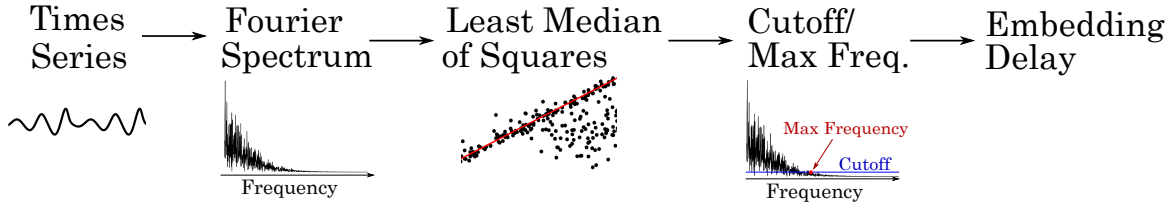


FIG. 5. Overview of our frequency domain approach for finding the maximum significant frequency  $f_{\max}$  using LMS for a signal contaminated with GWN.

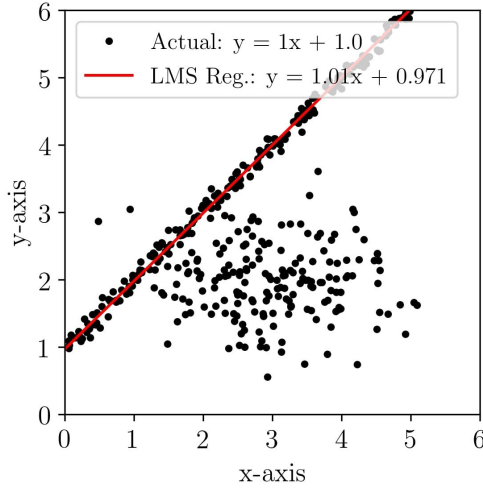


FIG. 6. LMS linear regression with 45% outliers. Results match those found in<sup>32</sup>.

Figure 9 shows embedding delays  $d_0$ ,  $d_1$ , and  $d_2$  calculated as  $d = \frac{\tau}{f_s}$  as well as their corresponding locations on a normalized MPE plot. This toy MPE plot shows that the normalized MPE reaches its first maximum when the delay is roughly  $d_1$ , which corresponds to approximately an even distribution of permutations. A second observation, as mentioned previously, is that at  $d_2$  (or the first dip in the MPE plot) there is a resonance or aliasing effect caused by  $\tau \approx \tau_r$ , which can be used to determine the period of the time series. This is based on the embedding delay size at  $d_2$  causing the embedding vector size  $V = d(n-1)$  to be approximately half the of the periodicity  $P$ , which can be expressed as

$$d_2 = \frac{1}{2}P = \frac{1}{f_s} \tau_r = \frac{1}{2f}, \quad (11)$$

where  $P$  is the main period of oscillation,  $f$  is the main frequency of the time series corresponding to  $P$ , and  $f_s$  is the sampling frequency. The reason for the dip in the permutation entropy (PE) when the condition from Eq. (11) is met is caused from an aliasing effect, which reduces PE through more regularity in the permutation distribution.

We use the criteria of Melosik and Marszalek<sup>34</sup> to determine a suitable delay from the location of the first dip at  $d_2$ . Their criteria states that the sampling frequency must fall within the range shown in Eq. (3). This range led to Eq. (4),

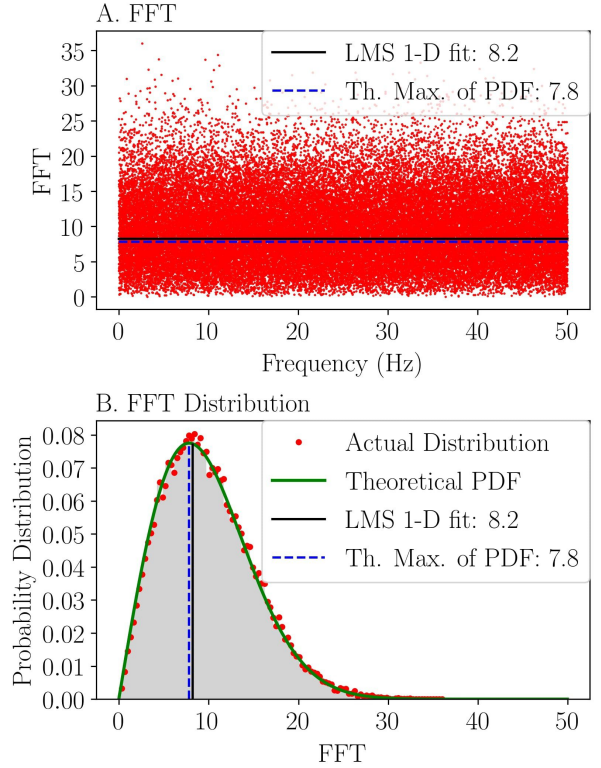


FIG. 7. (A) FFT of GWN with 0.035 standard deviation and zero mean with the location of the theoretical maximum of the PDF and one-dimensional LMS regression value. (B) Distribution of GWN in the Fourier Spectrum with overlapped theoretical PDF and location of the theoretical maximum of the PDF and one-dimensional LMS regression value.

which is used to calculate  $\tau$ . However, for MPE, we substitute  $f_s$  and  $f_{\max}$  in Eq. (3) with  $f_s = 2f\tau_r$  from Eq. (11) and  $f_{\max} = f$ . These substitutions allow Eq. (4) to reduce to

$$\tau = \frac{2}{\alpha} \tau_r, \quad (12)$$

where  $\alpha \in [2, 4]$ . These simplifications show that  $\tau$  is only dependent on the delay which causes resonance  $\tau_r$  when applying MPE. However, for a chaotic time series, the dip at  $\tau_r$  may not be present due to non-linear trends. To address this issue, we will first investigate the three dominant regions of the MPE plot, which will also be located for a chaotic time series example. We will then propose a new, automatic method

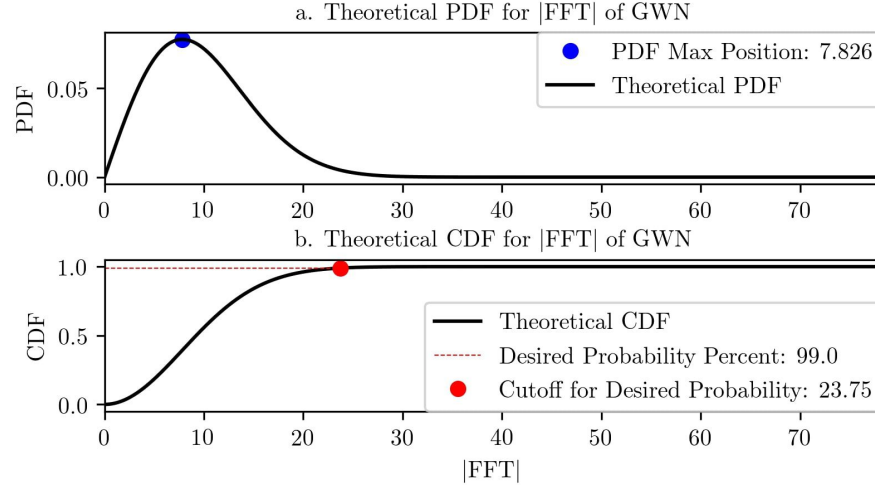


FIG. 8. (a) Theoretical PDF for GWN. (b) CDF for GWN with an example cutoff at the 99%  $CP$ .

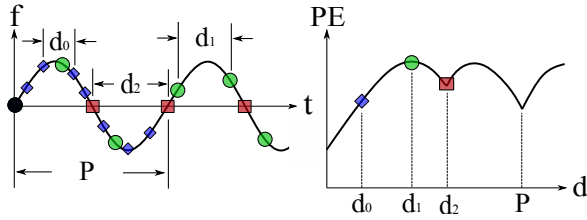


FIG. 9. (right) Resulting MPE plot for (left)  $2P$  periodic time series with example embedding delays  $d_0$ ,  $d_1$ , and  $d_2$ .

for selecting  $\tau$  that agrees with the frequency criteria stated in Eq. (12). Additionally, in Section A 2 b of the appendix we investigate the robustness of the method to noise and in Section A 5 of the appendix we provide the algorithm (Algorithm 1) for finding  $\tau$  using MPE.

*a. MPE Regions* Riedl et al.<sup>44</sup> showed that the MPE plot can be separated into three distinct regions as described below and shown in Fig. 10. Region A shows a gradual increase in the permutation entropy until reaching a maxima at the transition between regions A and B. Oversampling or a low value of  $\tau$  causes the motif distribution corresponding to the permutation entropy to be heavily weighted on just increasing or decreasing motifs (motifs (0,1,2) and (2,1,0) for  $n = 3$  from Fig. 2). This effect was coined as the “Redundancy Effect” by De Micco et al.<sup>17</sup>, which means sufficiently low values of  $\tau$  result in redundant motifs. However, as  $\tau$  increases, the motif distribution becomes more equiprobable. Additionally, when the motif probability reaches a maximum equiprobability, the permutation entropy is at a maxima, which is the point of transitions from region A to B. Region B shows a slight dip to the first minima. This reduction in permutation entropy is caused by the aliasing or resonance from the value of  $d$  approaching half the main period length. At the transition from B to C, the resonance is reached, which provides information on the main frequency and period of the time series. Region C has possible additional minima and maxima from additional alignment

of the embedding vector  $d$  with multiples of the main period. This region was referred to as the “Irrelevant Region” by De Micco et al.<sup>17</sup> due to effectively large values of  $\tau$  forcing the delayed sampling frequency to fall below the Nyquist sampling rate as described by the lower bound in Eq. (3).

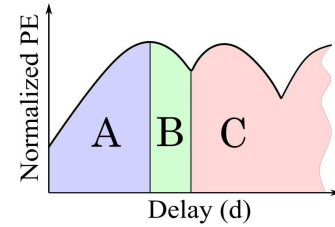


FIG. 10. The three regions of the MPE plot for a periodic signal: (A) redundant, (B) resonant, and (C) irrelevant.

*b. MPE Example with Chaotic Time Series* In Sections II B and II B 0 a, we used a periodic time series to show and explain the regions developed in an MPE plot as well as an MPE-based method for determining a suitable embedding delay  $\tau$ . In this section we further show the applicability of this approach to chaotic signals using the  $x$ -coordinate of the Lorenz System as an example. We simulate the Lorenz equations

$$\frac{dx}{dt} = \sigma(y - x), \quad \frac{dy}{dt} = x(\rho - z) - y, \quad \frac{dz}{dt} = xy - \beta z, \quad (13)$$

with a sampling rate of 100 Hz and using the parameters  $\rho = 28.0$ ,  $\sigma = 10.0$ , and  $\beta = 8.0/3.0$ . This system was solved for 100 seconds and only the last 15 seconds from the time series are used. Figure 11 shows the result of applying MPE to the simulated Lorenz system.

Figure 11 shows similarities to Fig. 10 with a clear maxima at the boundary between regions A and B, albeit with no obvious minima. Therefore, a new distinct feature needs to be used to determine  $\tau_r$ . We suggest using the first maxima

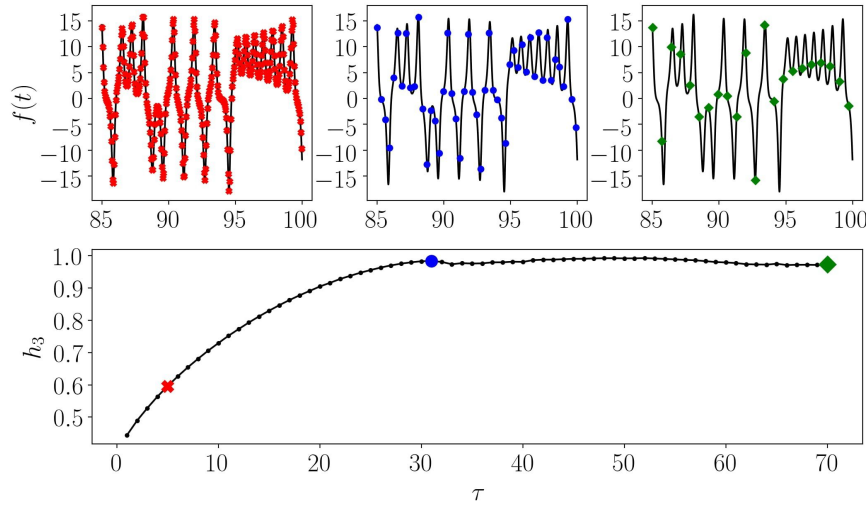


FIG. 11. MPE plot for the  $x$  coordinate of the Lorenz system. Additionally, points in the MPE plot with their corresponding subsampled time series are shown for the redundant, resonant, and irrelevant regions as described in Section II B 0 a.

to find  $\tau$  because this delay is likely to fall within the region described by Eq. (12).

### C. Autocorrelation for Embedding Delay

Autocorrelation is a traditional method for selecting  $\tau$  for phase space reconstruction by using the correlation coefficient between the time series and its  $\tau$ -lagged version. This method was first introduced by Box et al.<sup>8</sup> in 1970. Typically, the autocorrelation function is computed as a function of  $\tau$  and, as a rule of thumb, a suitable delay  $\tau$  is found when the correlation between  $x(t)$  and  $x(t + \tau)$  reaches the first folding time, i.e., when  $\rho \leq 1/e^{24}$ . The two prominent correlation techniques that are commonly used when implementing an autocorrelation-based approach for finding  $\tau$  are Pearson Correlation (see Section A 3 a of appendix) and Spearman's Correlation (see Section A 3 b of appendix). Additionally, an example demonstrating how to calculate  $\tau$  using autocorrelation and the difference between the two correlation methods is provided in Section A 3 c of the appendix.

### D. Mutual Information for Embedding Delay

Mutual information (MI) can be used to select the embedding delay  $\tau$  based on a minimum in the joint probability between two sequences. The mutual information between two discrete sequences was first realized by Shannon et al.<sup>45</sup> as

$$I(X;Y) = \sum_{x \in X} \sum_{y \in Y} p(x,y) \log \frac{p(x,y)}{p(x)p(y)}, \quad (14)$$

where  $X$  and  $Y$  are the two sequences,  $p(x)$  and  $p(y)$  are the probability of the element  $x$  and  $y$  separately, and  $p(x,y)$  is the joint probability of  $x$  and  $y$ . Fraser and Swinney<sup>20</sup> showed

that for a chaotic time series the MI between the original sequence  $x(t)$  and delayed version  $x(t + \tau)$  will decrease as  $\tau$  increases until reaching a first minimum. At this minima, the delay  $\tau$  allows for the individual data points to share a minimum amount of information, which indicates sufficiently separated data points. While this delay value was specifically developed for phase space reconstruction, it is also used for the selection of the PE parameter  $\tau$ . We would like to point out that, in general, there is no guarantee that local minima exist in the mutual information, which is a serious limitation for computing  $\tau$  using this method. All MI methods can be applied to either ranked or unranked data. We investigate four methods for estimating  $\tau$  for PE using MI. These methods include MI with equal-sized partitions, adaptive partitions, and two permutation-based MI estimation methods. For details on these methods please reference the appendix in Section A 4.

To determine the optimal MI approximation method for selecting  $\tau$  for PE, Table 12 shows a comparison between the  $\tau$  values computed from each of the MI methods and the corresponding values suggested by experts. The table shows that the adaptive partitioning method of Section A 4 b results in an accurate selection of  $\tau$  for the majority of systems. Therefore, we will use the adaptive partitioning estimation method when making comparisons to other methods. Additionally, for the exact values of  $\tau$  from each of the MI methods please reference Table I in the appendix.

### E. Permutation Auto-mutual Information for Selecting Delay

As shown in Section II D, Mutual information (MI) is a useful method for selecting  $\tau$  for phase space reconstruction. However, it does not account for the permutation distribution when selecting  $\tau$ , which can lead to inaccuracies in computing the PE. To circumvent this issue, we develop a new method for selecting  $\tau$  using Permutation Auto-Mutual Information



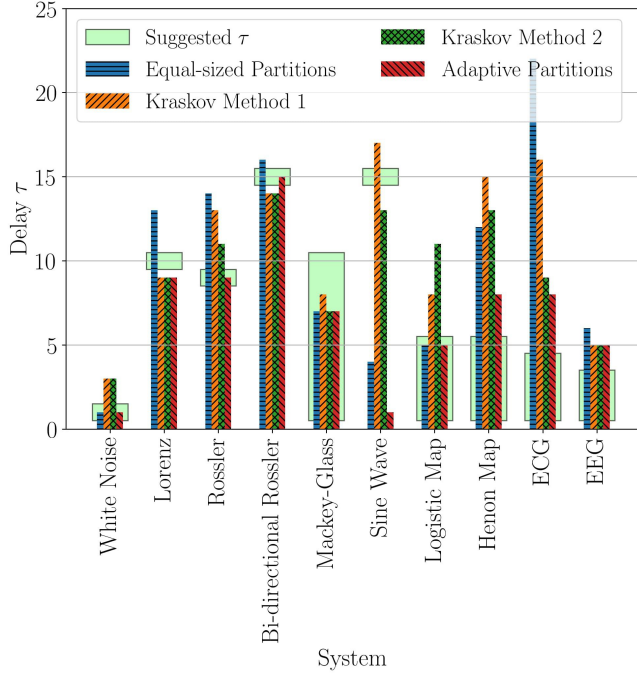


FIG. 12. A comparison between the calculated and suggested values for the delay parameter  $\tau$  for multiple MI approximation methods. The methods investigated were equal-sized partition method, Kraskov et al. methods 1 and 2, and the adaptive partitioning approach.

(PAMI). PAMI was first introduced by Liang et al.<sup>31</sup> as a tool for detecting dynamic changes in brain activity. In this paper we are tailoring PAMI for its application in the selection of the permutation entropy parameter  $\tau$  for the first time. This is done by measuring the joint probability between the original permutations formed when a delay of  $\tau = 1$  is used and to the permutations when  $\tau$  is incremented. PAMI is defined as

$$I_p(\tau, n) = H_{x(t, n)} + H_{x(t+\tau, n)} - H_{x(t, n), x(t+\tau, n)}, \quad (15)$$

where  $H$  is the permutation entropy described in Eq. (1). We suggest an optimal delay  $\tau$  for a given dimension  $n$  when PAMI is at a minimum. This delay corresponds to minimum shared information between the original permutations with  $\tau = 1$  and its time lagged permutations. By applying this method for the simple sinusoidal function described in Section A 5 e, we can form Fig. 13 with  $n \in [2, 5]$  and  $\tau \in [1, 50]$ . As shown, the window size is approximately independent of the dimension  $n$ , with an optimal window  $\tau(n-1) \approx 25$  for the example. Through our analysis of the minimum PAMI as a function of the window size, we have developed a new method for selecting the optimal embedding window. However, we need the embedding dimension to suggest an optimal delay. To do this, we implement the common choice for  $n$  ranging from  $4 \leq n \leq 6$  for PE<sup>44</sup>. To reduce the computational demand, we suggest using permutation dimensions  $n = 2$  to find an optimal window size. In addition to the reduced computational demand of using  $n = 2$ , we found that  $I_p(n = 2) \approx 0$  at the first minima. This also helps making this first minima

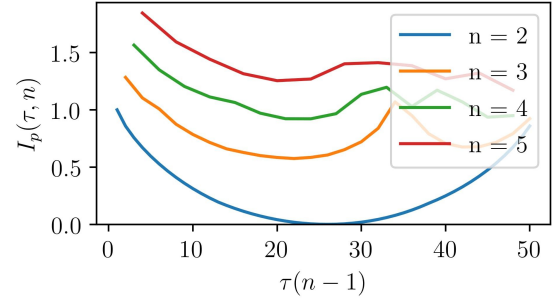


FIG. 13. PAMI results for the sinusoidal function described in Section A 5 e with  $n \in [2, 5]$  and  $\tau \in [1, 50]$ . The figure shows an optimal window size  $\tau(n-1) \approx 25$ .

even more simple.

### III. METHODS FOR MOTIF DIMENSION

The second parameter for permutation entropy that needs to be automatically identified is the embedding dimension  $n$ . The methods for determining  $n$  fall into one of two categories: (1) independently determining  $n$  and  $\tau$ , and (2) simultaneously determining  $n$  and  $\tau$  based on the width of the embedding window. For the first category, we investigate using the method of False Nearest Neighbors (FNN)<sup>25</sup> in Section III A, and Singular Spectrum Analysis (SSA)<sup>9</sup> in Section III B. For the second category, we contribute to the selection of  $n$  by developing an automatic method using MPE from Section III C. This method combines the results for finding  $\tau$  through MPE in Section II B with the work of Riedl et al.<sup>44</sup>. We recognize that our work does not include other commonly used methods for independently calculating  $n$  such as box-counting<sup>13</sup>, largest Lyapunov exponent<sup>51</sup>, and Kolmogorov–Sinai entropy<sup>38</sup>.

#### A. False Nearest Neighbors for Embedding Dimension

False Nearest Neighbors (FNN) is one of the most commonly used methods for determining the minimum embedding dimension  $n$  for state space reconstruction. It was originally developed by Kennel et al.<sup>25</sup> as a geometric approach for determining the minimum needed embedding dimension. In this method the time series is repeatedly embedded into an a sequence of  $m$ -dimensional Euclidean spaces for a range of increasing values of  $m$ . The idea is that when the minimum embedding dimension  $m$  is reached or  $m \geq n$ , the distance between neighboring points does not significantly change as we keep increasing  $m$ . In other words, the Euclidean distance  $d_m(i, j)$  between the point  $\mathbf{P}_i \in \mathbb{R}^m$  and its nearest neighbor  $\mathbf{P}_j \in \mathbb{R}^m$  minimally changes when the embedding dimension increases to  $m+1$ . If the dimension  $m$  is not sufficiently high, then the points are false neighbors if their pairwise distance significantly increases when incrementing  $m$ . This ratio of change in the distance between nearest neighbors embedded in  $\mathbb{R}^m$  and  $\mathbb{R}^{m+1}$  is quantified using the ratio of false nearest

neighbors

$$R_i = \sqrt{\frac{d_{m+1}^2(i, j) - d_m^2(i, j)}{d_m^2(i, j)}}. \quad (16)$$

$R_i$  is compared to the tolerance threshold  $R_{\text{tol}}$  to distinguish false neighbors when  $R_i > R_{\text{tol}}$ . In this paper, we select  $R_{\text{tol}} = 15$  as used by Kennel et al.<sup>25</sup>. By applying this threshold over all points, we can find the number of false neighbors as a percent FNN  $P_{\text{FNN}}$ . If there is no noise in the system,  $P_{\text{FNN}}$  should reach zero when a sufficient dimension is reached. However, with additive noise present,  $P_{\text{FNN}}$  may never reach zero. Thus, it is commonly suggested to use a percent FNN cutoff for finding a sufficient dimension  $n$ . We use the typically chosen cutoff  $P_{\text{FNN}} < 10\%$ , which is suitable for most applications when moderate noise is present.

### B. Singular Spectrum Analysis for Embedding Dimension

The singular spectrum analysis method was first introduced by Broomhead and King<sup>9</sup> as a tool to find the trends and most prominent periods of a time series. Leles et al.<sup>29</sup> summarized the SSA procedure as (1) immersion, (2) Singular Value Decomposition (SVD), (3) grouping, and (4) diagonal averaging. Specifically, immersion embeds the time series into a dimension  $L$  to form a Hankel matrix, SVD factors all the matrices, grouping combines the matrices that are similar in structure, and diagonal averaging reconstructs the time-series using the combined matrices. The needed embedding dimension is determined from the SVD by calculating the ratio  $D$

$$D = \frac{g_L}{g_r} \quad (17)$$

of the sum of the  $L$ th diagonal entries  $g_L$  to the sum of the total diagonal entries  $g_r$ . When  $D$  exceeds 0.9, we consider the dimension to be high enough and set  $n = L$ , which can then be used as the embedding dimension for permutation entropy.

### C. Multi-scale Permutation Entropy for Permutation Dimension

Riedl et al.<sup>44</sup> showed how MPE can be used to determine an embedding dimension  $n$ . This method requires the embedding delay  $\tau$  to be set to the length of the main period of the signal as shown in Section II B. The theory behind the method is based on normalizing the MPE according to

$$h'_n = \frac{-1}{n-1} H(n), \quad (18)$$

where  $h'_n$  is the PE normalized using the embedding dimension, and  $H_n$  is the PE calculated from Eq. (1). Riedl et al.<sup>44</sup> determine the embedding dimension by incrementing  $n$  to find the largest corresponding normalized PE  $h'_n$  with an embedding delay  $\tau$  heuristically determined from the main period length. They concluded that the  $h'_n$  with the highest entropy

accurately accounts for the needed complexity of the time series, and therefore suggests a suitable embedding dimension. Riedl et al.<sup>44</sup> show how this method provides an accurate embedding dimension for the Van-der-Pol-oscillator, Lorenz system, and the logistic map. However, the method is not automatic due to the reliance on a heuristically chosen  $\tau$ .

To make the process automatic, we introduce algorithm 1 based on Section II B to automatically select the correct  $\tau$ , which we then use in conjunction with Eq. (18) to find  $n$  corresponding to the maximum  $h'_n$ . Additionally, we suggest scaling  $n$  from 3 to 8 as we have not yet found a system requiring  $n > 8$  using this method.

## IV. RESULTS AND DISCUSSION

To make conclusions about the described methods for determining  $\tau$  and  $n$ , we made comparisons to values suggested by experts. The majority of the suggested parameters are taken from the work of Riedl et al.<sup>44</sup>, while parameters for the Rossler system and sine wave are from Tao et al.<sup>50</sup>. Figures 14 and 15 show the calculated and suggested values for  $\tau$  and  $n$ , respectively. For the exact values of  $\tau$  and  $n$  from each of the parameter estimation methods please reference Tables II and III in the appendix, respectively. Additionally, script for reproducing the results found in this paper are provided through the Mendeley.

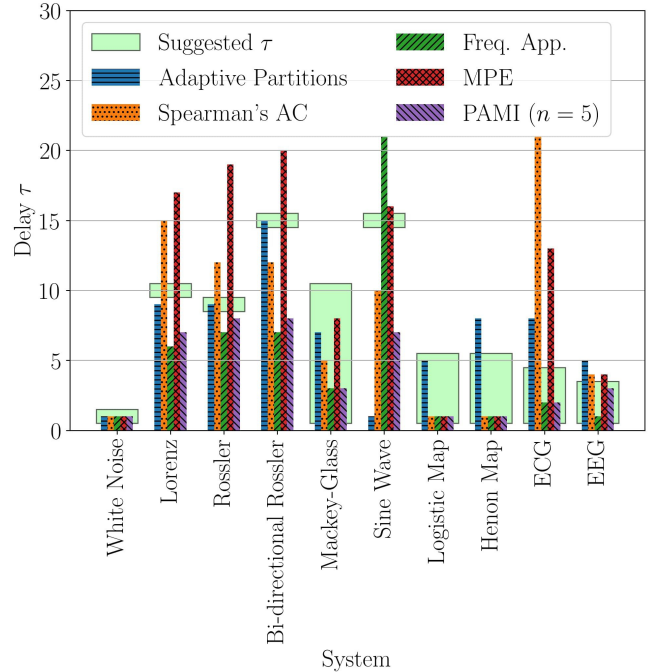


FIG. 14. A comparison between the calculated and suggested values for the delay parameter  $\tau$ . The methods investigated were MI with adaptive partitions, Spearman's Autocorrelation (AC), the frequency analysis, Multi-scale Permutation Entropy (MPE), and Permutation Auto-mutual Information (PAMI) with  $n = 5$ .

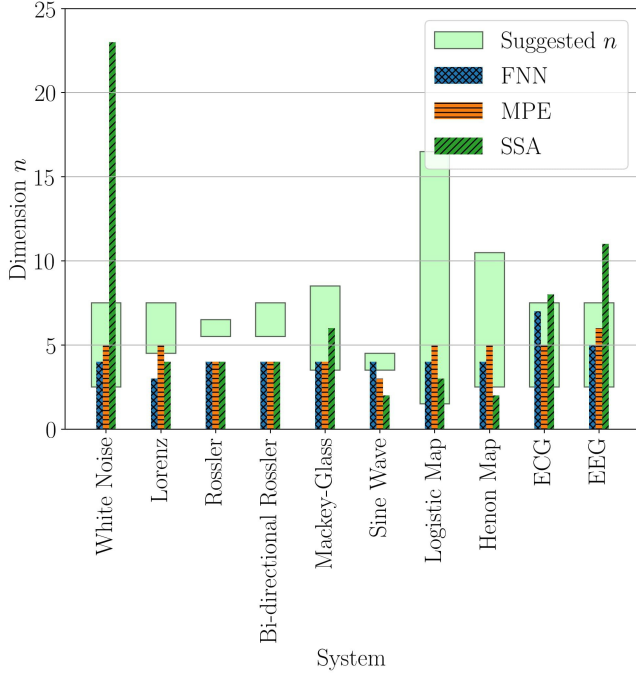


FIG. 15. A comparison between the calculated and suggested values for the embedding dimension  $n$ . The methods investigated were False Nearest Neighbors (FNN), Multi-scale Permutation Entropy (MPE), and Singular Spectrum Analysis (SSA).

*a. Embedding Delay* Figure 14 shows the automatically computed  $\tau$  in comparison to the expert-identified values for a variety of systems. These systems fall within several categories including the following: noise, chaotic differential equations, periodic systems, nonlinear difference equations, and medical data. The methods presented in Fig. 14 include PAMI from Section II E, MI calculated using adaptive partitioning from Section A 4 b, Spearman’s Autocorrelation from Section II C, MPE from Section II B, and the frequency approach from Section II A. For the noise category we only investigated Gaussian white noise, and all the methods accurately suggest an embedding delay. For the second category of chaotic differential equations, Mutual Information approximated using adaptive partitions accurately provided suitable delay values. However, as addressed in Section I, there are possible modes of failure for MI. To validate that MI is accurately selecting a value for  $\tau$ , we recommend also calculating  $\tau$  using the frequency approach. For the third category, periodic systems, we only investigated a simple sinusoidal function. This resulted in both MPE and the Frequency approach providing accurate suggestions. Therefore, we suggest using both of these methods to calculate  $\tau$  for periodic systems. Additionally, we do not suggest the use of MI for periodic systems as it can have early false minima resulting in inaccurate delay selection. For difference equations we found that PAMI, autocorrelation, MPE, and the frequency approach provide accurate suggestions for the delay. Finally, when testing each method on medical data with intrinsic noise, we found that the noise-robust frequency approach yielded the optimal

parameter selection for  $\tau$ . As a generalization of the results found, we suggest the use of MI with adaptive partitioning when selecting  $\tau$  for chaotic differential equations. For periodic systems, nonlinear difference equations, and ECG/EEG data we suggest the use of the frequency approach that we developed in this paper. However, when applying the frequency approach to quasiperiodic time series with multiple harmonics of decreasing amplitude, the method may fail due to the delay being selected based on an insignificant high frequency. The use of either Spearman’s autocorrelation or MPE may be more suitable under this condition. In general, multiple methods should be used for each system to validate that an accurate delay is selected due to the possible modes of failure of each method. Specifically, The frequency approach may fail if the noise does not have a Gaussian distribution, MI can fail if a false minima occurs or the relationship is monotonic, and autocorrelation can fail if the time series being analyzed does not oscillate about a fixed value.

*b. Embedding Dimension* Figure 15 shows the automatically computed parameter  $n$  in comparison to the expert-identified values. It can be seen that both MPE and FNN commonly had parameters within the range specified for all categories. However, SSA failed to provide a consistently suitable embedding dimension  $n$ . This leads to the conclusion that either MPE or FNN are sufficient methods for determining the embedding dimension for the majority of the considered applications. However, FNN may fail if the effects of noise are not correctly accounted for, which can lead to overly large embedding dimensions. These results also show that the dimension  $n = 6$  works well for almost all applications.

## V. CONCLUSION

In this paper we demonstrated various methods for automatically determining the PE parameters  $\tau$  and  $n$  when supplied with a sufficiently sampled/oversampled time series. The goal is to find, in an automatic way, the most accurate method in comparison to expert suggested parameters. The methods we investigated for calculating  $\tau$  include autocorrelation, mutual information, permutation-auto-mutual information, frequency analysis, and multi-scale permutation entropy. Additionally, the methods we investigated for determining the embedding dimension  $n$  include false nearest neighbors, singular spectrum analysis, and multiscale permutation entropy. Several of these methods for calculating  $\tau$  or  $n$  do have suggested parameters to be set by hand. This leaves some methods as not completely automatic. However, the methods of MI, autocorrelation, MPE, and PAMI do not have any parameters set, which reduces the user influence on parameter selection and improves the automatic selection. Additionally, the parameters that are suggested are default parameters that work for the majority of applications.

Our first contribution was developing a new frequency approach analysis and extending two existing methods, PAMI, and MPE, to automatically determine  $\tau$ . For the frequency approach, we developed an automatic algorithm for finding the maximum significant frequency using a cutoff greater than the

noise floor. The noise floor was found using one dimensional least median of squares applied to the Fourier spectrum in conjunction with the theoretical probability distribution function for the Fourier transform of Gaussian white noise. For PAMI, we showed how the minimum in the PAMI can be used to find an optimal embedding window, which is approximately independent of the dimension  $n$ . We then suggested using the range  $4 \leq n \leq 6$  to find  $\tau$  from the first minima in PAMI for  $n = 2$ . For MPE, we showed how it can be used to find the main period of oscillation from a periodic time series, which we then use to find  $\tau$ . Additionally, we expanded upon this method by showing how the main period of oscillation can also be found for non-periodic time series, which we implemented into an automatic algorithm.

Our second contribution was implementing the automatic selection of  $\tau$  using MPE to also find  $n$  using MPE. We also collected and compared some of the most popular methods for obtaining  $n$  including false nearest neighbors, and singular spectrum analysis. We applied these methods to various categories including difference equations, chaotic differential equations, periodic systems, EEG/ECG data, and Gaussian noise. We then compared the generated parameters to values suggested by experts to determine which methods consistently found accurate values for  $\tau$  and  $n$ . We found that SSA did not provide suitable values for  $n$ . However, both FNN and MPE provided accurate values for  $n$  for most of the systems. We also concluded that, for the majority applications, a permutation dimension  $n = 5$  is suitable. For determining  $\tau$ , we showed that our frequency approach provided accurate suggestions for  $\tau$  for periodic systems, nonlinear difference equations, and medical data, while the mutual information function computed using adaptive partitions provided the most accurate results for chaotic differential equations.

## ACKNOWLEDGMENT

FAK acknowledges the support of the National Science Foundation under grants CMMI-1759823 and DMS-1759824.

- <sup>1</sup>José M. Amigó, Roberto Monetti, Thomas Aschenbrenner, and Wolfram Bunk. Transcripts: An algebraic approach to coupled time series. *Chaos: An Interdisciplinary Journal of Nonlinear Science*, 22(1):013105, mar 2012.
- <sup>2</sup>Ralph G Andrzejak, Klaus Lehnertz, Florian Mormann, Christoph Rieke, Peter David, and Christian E Elger. Indications of nonlinear deterministic and finite-dimensional structures in time series of brain electrical activity: Dependence on recording region and brain state. *Physical Review E*, 64(6):061907, 2001.
- <sup>3</sup>Massoud Babaie-Zadeh and Christian Jutten. A general approach for mutual information minimization and its application to blind source separation. *Signal Processing*, 85(5):975–995, may 2005.
- <sup>4</sup>Christoph Bandt and Bernd Pompe. Permutation entropy: a natural complexity measure for time series. *Physical review letters*, 88(17):174102, 2002.
- <sup>5</sup>Aurelio F. Bariviera, Luciano Zunino, and Osvaldo A. Rosso. An analysis of high-frequency cryptocurrencies prices dynamics using permutation-information-theory quantifiers. *Chaos: An Interdisciplinary Journal of Nonlinear Science*, 28(7):075511, jul 2018.
- <sup>6</sup>T. Berry, J. R. Cressman, Z. Gregurić-Ferenčak, and T. Sauer. Time-scale separation from diffusion-mapped delay coordinates. *SIAM Journal on Applied Dynamical Systems*, 12(2):618–649, jan 2013.
- <sup>7</sup>A Block, W Von Bloh, and HJ Schellnhuber. Efficient box-counting determination of generalized fractal dimensions. *Physical Review A*, 42(4):1869, 1990.
- <sup>8</sup>George EP Box, Gwilym M Jenkins, Gregory C Reinsel, and Greta M Ljung. *Time series analysis: forecasting and control*. John Wiley & Sons, 2015.
- <sup>9</sup>David S Broomhead and Gregory P King. Extracting qualitative dynamics from experimental data. *Physica D: Nonlinear Phenomena*, 20(2-3):217–236, 1986.
- <sup>10</sup>Th Buzug and G Pfister. Optimal delay time and embedding dimension for delay-time coordinates by analysis of the global static and local dynamical behavior of strange attractors. *Physical review A*, 45(10):7073, 1992.
- <sup>11</sup>Yinhe Cao, Wen-wen Tung, JB Gao, Vladimir A Protopopescu, and Lee M Hively. Detecting dynamical changes in time series using the permutation entropy. *Physical review E*, 70(4):046217, 2004.
- <sup>12</sup>Yu-Min Chung, Chuan-Shen Hu, Yu-Lun Lo, and Hau-Tieng Wu. A persistent homology approach to heart rate variability analysis with an application to sleep-wake classification. *arXiv preprint arXiv:1908.06856*, 2019.
- <sup>13</sup>Septima Poinsette Clark. Estimating the fractal dimension of chaotic time series. *Lincoln Laboratory Journal*, 3(1), 1990.
- <sup>14</sup>Madalena Costa, Ary L Goldberger, and C-K Peng. Multiscale entropy analysis of complex physiologic time series. *Physical review letters*, 89(6):068102, 2002.
- <sup>15</sup>Thomas M Cover and Joy A Thomas. *Elements of information theory*. John Wiley & Sons, 2012.
- <sup>16</sup>G.A. Darbellay and I. Vajda. Estimation of the information by an adaptive partitioning of the observation space. *IEEE Transactions on Information Theory*, 45(4):1315–1321, may 1999.
- <sup>17</sup>Luciana De Micco, Juana Graciela Fernández, Hilda A Larrondo, Angelo Plastino, and Osvaldo A Rosso. Sampling period, statistical complexity, and chaotic attractors. *Physica A: Statistical Mechanics and its Applications*, 391(8):2564–2575, 2012.
- <sup>18</sup>Bin Deng, Li Liang, Shunan Li, Ruofan Wang, Haitao Yu, Jiang Wang, and Xile Wei. Complexity extraction of electroencephalograms in alzheimers disease with weighted-permutation entropy. *Chaos: An Interdisciplinary Journal of Nonlinear Science*, 25(4):043105, apr 2015.
- <sup>19</sup>Birgit Frank, Bernd Pompe, Uwe Schneider, and Dirk Hoyer. Permutation entropy improves fetal behavioural state classification based on heart rate analysis from biomagnetic recordings in near term fetuses. *Medical and Biological Engineering and Computing*, 44(3):179, 2006.
- <sup>20</sup>Andrew M Fraser and Harry L Swinney. Independent coordinates for strange attractors from mutual information. *Physical review A*, 33(2):1134, 1986.
- <sup>21</sup>Joshua Garland, Tyler Jones, Michael Neuder, Valerie Morris, James White, and Elizabeth Bradley. Anomaly detection in paleoclimate records using permutation entropy. *Entropy*, 20(12):931, 2018.
- <sup>22</sup>Joshua Garland, Tyler R Jones, Elizabeth Bradley, Michael Neuder, and James WC White. Climate entropy production recorded in a deep antarctic ice core. *arXiv preprint arXiv:1806.10936*, 2018.
- <sup>23</sup>Peter Grassberger and Itamar Procaccia. Measuring the strangeness of strange attractors. *Physica D: Nonlinear Phenomena*, 9(1-2):189–208, 1983.
- <sup>24</sup>Holger Kantz and Thomas Schreiber. *Nonlinear time series analysis*, volume 7. Cambridge university press, 2004.
- <sup>25</sup>Matthew B Kennel, Reggie Brown, and Henry DI Abarbanel. Determining embedding dimension for phase-space reconstruction using a geometrical construction. *Physical review A*, 45(6):3403, 1992.
- <sup>26</sup>Alexander Kraskov, Harald Stögbauer, and Peter Grassberger. Estimating mutual information. *Physical Review E*, 69(6), jun 2004.
- <sup>27</sup>HJ Landau. Sampling, data transmission, and the nyquist rate. *Proceedings of the IEEE*, 55(10):1701–1706, 1967.
- <sup>28</sup>David Lane, Joan Lu, Camille Peres, Emily Zitek, et al. Online statistics: An interactive multimedia course of study. *Retrieved January*, 29:2009, 2008.
- <sup>29</sup>Michel CR Leles, João Pedro H Sansão, Leonardo A Mozelli, and Homero N Guimarães. Improving reconstruction of time-series based in singular spectrum analysis: A segmentation approach. *Digital Signal Pro-*

- cessing, 77:63–76, 2018.
- <sup>30</sup>Duan Li, Zhenhu Liang, Yinghua Wang, Satoshi Hagihira, Jamie W. Sleight, and Xiaoli Li. Parameter selection in permutation entropy for an electroencephalographic measure of isoflurane anesthetic drug effect. *Journal of Clinical Monitoring and Computing*, 27(2):113–123, dec 2012.
- <sup>31</sup>Zhenhu Liang, Yinghua Wang, Gaoxiang Ouyang, Logan J Voss, Jamie W Sleight, and Xiaoli Li. Permutation auto-mutual information of electroencephalogram in anesthesia. *Journal of Neural Engineering*, 10(2):026004, feb 2013.
- <sup>32</sup>Desire L Massart, Leonard Kaufman, Peter J Rousseeuw, and Annick Leroy. Least median of squares: a robust method for outlier and model error detection in regression and calibration. *Analytica Chimica Acta*, 187:171–179, 1986.
- <sup>33</sup>Michael McCullough, Michael Small, Thomas Stemler, and Herbert Ho-Ching Iu. Time lagged ordinal partition networks for capturing dynamics of continuous dynamical systems. *Chaos: An Interdisciplinary Journal of Nonlinear Science*, 25(5):053101, 2015.
- <sup>34</sup>Michał Melosik and W Marszałek. On the 0/1 test for chaos in continuous systems. *Bulletin of the Polish Academy of Sciences Technical Sciences*, 64(3):521–528, 2016.
- <sup>35</sup>George B Moody and Roger G Mark. The impact of the mit-bih arrhythmia database. *IEEE Engineering in Medicine and Biology Magazine*, 20(3):45–50, 2001.
- <sup>36</sup>Audun Myers, Elizabeth Munch, and Firas A Khasawneh. Persistent homology of complex networks for dynamic state detection. *arXiv preprint arXiv:1904.07403*, 2019.
- <sup>37</sup>Athanasios Papoulis and S Unnikrishna Pillai. *Probability, random variables, and stochastic processes*. Tata McGraw-Hill Education, 2002.
- <sup>38</sup>Yakov Borisovich Pesin. Characteristic lyapunov exponents and smooth ergodic theory. *Uspekhi Matematicheskikh Nauk*, 32(4):55–112, 1977.
- <sup>39</sup>Steven M Pincus. Approximate entropy as a measure of system complexity. *Proceedings of the National Academy of Sciences*, 88(6):2297–2301, 1991.
- <sup>40</sup>Anton Popov, Oleksii Avilov, and Oleksii Kanaykin. Permutation entropy of eeg signals for different sampling rate and time lag combinations. In *Signal Processing Symposium (SPS)*, 2013, pages 1–4. IEEE, 2013.
- <sup>41</sup>Alberto Porta, Vlasta Bari, Andrea Marchi, Beatrice De Maria, Paolo Castiglioni, Marco di Rienzo, Stefano Guzzetti, Andrei Cividjian, and Luc Quintin. Limits of permutation-based entropies in assessing complexity of short heart period variability. *Physiological Measurement*, 36(4):755–765, mar 2015.
- <sup>42</sup>Mark A Richards. The discrete-time fourier transform and discrete fourier transform of windowed stationary white noise. *Georgia Institute of Technology, Tech. Rep*, 2013.
- <sup>43</sup>Joshua S Richman and J Randall Moorman. Physiological time-series analysis using approximate entropy and sample entropy. *American Journal of Physiology-Heart and Circulatory Physiology*, 278(6):H2039–H2049, 2000.
- <sup>44</sup>Müller Riedl, A Müller, and N Wessel. Practical considerations of permutation entropy. *The European Physical Journal Special Topics*, 222(2):249–262, 2013.
- <sup>45</sup>Claude E Shannon, Warren Weaver, and Arthur W Burks. The mathematical theory of communication. 1951.
- <sup>46</sup>Claude Elwood Shannon. A mathematical theory of communication. *ACM SIGMOBILE mobile computing and communications review*, 5(1):3–55, 2001.
- <sup>47</sup>Matthaus Staniek and Klaus Lehnertz. Parameter selection for permutation entropy measurements. *International Journal of Bifurcation and Chaos*, 17(10):3729–3733, oct 2007.
- <sup>48</sup>Herbert A Sturges. The choice of a class interval. *Journal of the american statistical association*, 21(153):65–66, 1926.
- <sup>49</sup>Floris Takens. Detecting strange attractors in turbulence. In *Dynamical systems and turbulence, Warwick 1980*, pages 366–381. Springer, 1981.
- <sup>50</sup>Mei Tao, Kristina Poskuvienė, Nizar Alkayem, Maosen Cao, and Minvydas Ragulskis. Permutation entropy based on non-uniform embedding. *Entropy*, 20(8):612, 2018.
- <sup>51</sup>Alan Wolf, Jack B Swift, Harry L Swinney, and John A Vastano. Determining lyapunov exponents from a time series. *Physica D: Nonlinear Phenomena*, 16(3):285–317, 1985.
- <sup>52</sup>Hong Zhang and Xuncheng Liu. Analysis of parameter selection for permutation entropy in logistic chaotic series. In *Intelligent Transportation, Big Data & Smart City (ICITBS), 2018 International Conference on*, pages 398–402. IEEE, 2018.
- <sup>53</sup>Luciano Zunino, Miguel C Soriano, Ingo Fischer, Osvaldo A Rosso, and Claudio R Mirasso. Permutation-information-theory approach to unveil delay dynamics from time-series analysis. *Physical Review E*, 82(4):046212, 2010.



## Appendix A: Appendix

### 1. PE Calculation Example

To demonstrate how PE is calculated, consider another sequence  $X = [4, 7, 9, 10, 6, 11, 3, 2]$  with PE parameters  $n = 3$  and  $\tau = 1$ . The left side of Fig 16 shows how the sequence can be broken down into the following permutations: two  $(0, 1, 2)$ , one  $(1, 0, 2)$ , two  $(1, 2, 0)$ , and one  $(2, 1, 0)$  for a total of 6 permutations. This makes each permutation type have a probability out of 6. The permutation distribution can be visually understood by illustrating the probabilities of each permutation as separate bins. To accomplish this, the right side of Fig. 16 shows the abundance of each permutation. Applying Eq. (1) to the probabilities of each permutation for our example sequence  $X$  yields

$$H(3) = -\frac{2}{5} \log \frac{2}{5} - \frac{2}{5} \log \frac{2}{5} - \frac{1}{5} \log \frac{1}{5} - \frac{1}{5} \log \frac{1}{5} = 1.918 \text{ bits.}$$

### 2. MPE Algorithm and Effects of Noise

#### a. MPE delay Algorithm

In Section II B 0 b we showed that choosing  $\tau$  using MPE should be based on the position of the first peak after the noise in the MPE plot for an embedding dimension of  $n = 3$ . At this maximum, the normalized PE hits a maximum of approximately 1. From this methodology, we developed Algorithm 1 to determine the delay  $\tau$  using the location of the first peak, while ignoring the noise region in Fig. 17.

**Result:**  $\tau$

```

begin
  set  $n = 3$ ;
  start with a delay of  $\tau = 1$ ;
  start with initial normalized PE as  $h_0 = 0$ ;
  while first peak not found do
    calculate normalized PE as  $h(\tau)$ ;
    if  $h(\tau) < 0.9$  then
      | Set outside of noise section flag as true ( $f_n = \text{True}$ )
    end
    if  $h(\tau) > 0.9$  and  $f_n = \text{True}$  then
      if  $h(\tau) < h_0$  then
        |  $\tau = \tau - 1$ ;
        | First peak found;
      end
      Set  $h_0 = h(\tau)$ 
    end
     $\tau = \tau + 1$ 
  end
  return  $\tau$ ;
end

```

**Algorithm 1:** Algorithm using MPE for  $\tau$ .

#### b. Effects of Noise

We found that the main advantage of using MPE for determining the embedding delay is its robustness to noise. Noise on an MPE plot has minimal effects on regions B and C from Fig. 10, while only significantly affecting region A as shown in Fig 17. Furthermore, depending on the signal to noise ratio, there will only be an effect at the beginning of region A. Figure 17 shows the first region N where noise is affecting the permutation entropy. The effect of noise causes the MPE plot to start at a maxima and decrease to a local minima. When the time delay becomes large enough, the permutations are no longer influenced by the noise causing this minima. We found that the location of the minima is based on the condition

$$m_{\text{avg}} \tau_N \approx A_{\text{noise}} f_s, \quad (\text{A1})$$

where  $m_{\text{avg}}$  is the average of the absolute value of the slope and  $A_{\text{noise}}$  is approximately the maximum amplitude of the noise,  $\tau_N$  is the value of  $\tau$  great enough to surpass the noise amplitude. We derived this condition from the need for, on average,  $|f(t) - f(t + \tau)| > A_{\text{noise}}$ . This shows that MPE is robust to noise as long as the noise amplitude does not exceed the amplitude of the signal.

### 3. Autocorrelation Methods and Example

#### a. Pearson Correlation

The Pearson correlation coefficient  $\rho_{xy} \in [-1, 1]$  measures the linear correlation of two time series  $x$  and  $y$ . Using these two data sets the correlation coefficient is calculated as

$$\rho_{xy} = \frac{\sum_{i=1}^n (x_i - \bar{x})(y_i - \bar{y})}{\sqrt{\sum_{i=1}^n (x_i - \bar{x})^2} \sqrt{\sum_{i=1}^n (y_i - \bar{y})^2}}. \quad (\text{A2})$$

The possible values of  $\rho_{xy}$  represent the relationship between the two data sets, where  $\rho_{xy} = 1$  represents a perfect positive linear correlation,  $\rho_{xy} = 0$  represents no linear correlation, while  $\rho_{xy} = -1$  represents a perfect negative linear correlation. However, Pearson correlation is limited because it only detects linear correlations. This limitation is somewhat alleviated by using Spearman's Correlation which operates on the ordinal ranking of the two time series instead of their numeric values.

#### b. Spearman's Correlation

Spearman's correlation is also calculated using Eq. (A2) with the substitution of  $x$  and  $y$  for their ordinal ranking. This substitution allows for detecting nonlinear correlation trends to be represented as long as the correlation is monotonic. To demonstrate the difference, Fig. 18 shows two sequences  $x$  and  $y$  calculated from  $y = x^4$  with  $x \in [0, 10]$ . Using this example, the Pearson correlation is calculated as  $\rho \approx 0.86$ , while Spearman's ranked correlation yields  $\rho = 1.0$ . This result

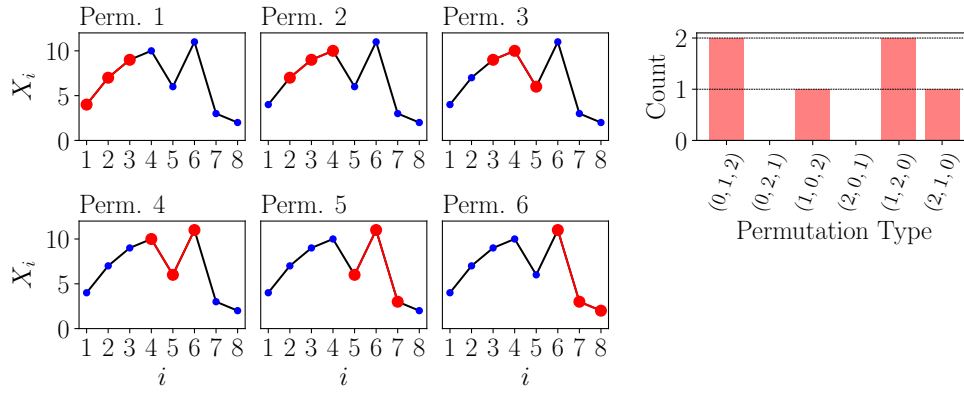


FIG. 16. Permutations 1 through 6 shown for example sequence  $X$  (left) with  $n = 3$  and  $\tau = 1$  and the relative abundance of each permutation (right). Permutation 1 corresponds to a  $(0, 1, 2)$ , permutation 2 is of type  $(0, 1, 2)$ , permutation 3 is of type  $(1, 2, 0)$ , permutation 4 is of type  $(1, 0, 2)$ , permutation 5 is of type  $(1, 2, 0)$ , and permutation 6 is of type  $(2, 1, 0)$ .

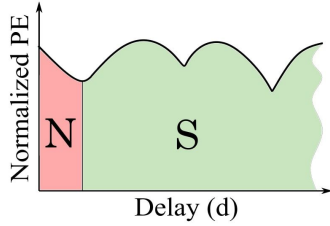


FIG. 17. Region N is affected by noise in the MPE plot, and region S is unaffected.

demonstrates how Spearman's correlation coefficient accurately detects the non-linear, monotonic correlation between  $x$  and  $y$  whereas Pearson correlation may miss it.

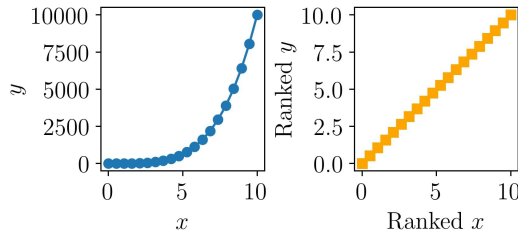


FIG. 18. A comparison between (left) unranked values and (right) ranked values for calculating correlation coefficients. Using the ranked  $x$  and  $y$ , Spearman's correlation coefficient can be used to accurately reveal existing nonlinear monotonic correlations.

### c. Autocorrelation Example

We can use the concept of correlation to select a delay  $\tau$  by calculating the correlation coefficient using Eq. (A2) between a time series and its  $\tau$ -lagged version. As an example, take the time series  $x(t) = \sin(2\pi t)$ , with  $t \in [0, 5]$  having a sampling frequency of 100 Hz. This results in a suggested de-

lay  $\tau = 20$  at the first folding time using both Spearman's and Pearson correlation. In section IV we will implement Spearman's version of autocorrelation to account for the possibility of non-linear correlations.

## 4. MI methods

### a. MI using Equal-sized Partitions

For the calculation of MI, the joint and independent probabilities of the original  $x(t)$  and time lagged  $x(t + \tau)$  time series are needed. However, since  $x$  is a discrete time series, we approximate these probabilities using bins, which segment the range of the series into discrete groups. The simplest method for approximating the probabilities using this discretization method is to use equal sized bins. However, the size of these bins is dependent on the number of bins  $k$ . We investigated various methods for estimating an appropriate number of bins using the length of the time series  $N$ . These methods include the common square-root choice  $k = \lceil \sqrt{N} \rceil$ , Sturge's formula<sup>48</sup>  $k = \lceil \log_2(N) \rceil + 1$ , and Rice Rule<sup>28</sup>  $k = \lceil 2N^{1/3} \rceil$ . After comparing each method using a variety of examples, we found that the use of Sturge's formula provided the best results for selecting  $\tau$  for PE using MI.

### b. MI using Adaptive Partitions

Darbellay and Vajda<sup>16</sup> introduced a multistep, adaptive partitioning scheme to select appropriate binning sizes in the observation space formed by the plane  $x(t)$  and  $x(t + \tau)$ . Their method is often considered state-of-the-art for estimating the mutual information function<sup>26</sup>. In this approach, the bins are recursively created where in the first function call, the space of the signal and its  $\tau$ -lagged version is divided into an equal number of 2D bins. Then a chi-squared test is used to test the null hypothesis that the data within the newly created bins are independent. Any segment that fails the test is further

divided until the resulting sub-segments contain independent data (or a certain number of divisions is satisfied). Using this partitioning method, the MI is calculated using Eq. (14).

### c. Kraskov MI

Kraskov et al.<sup>26</sup> developed a method for approximating the MI using entropy estimates using partition sizes based on  $k$ -nearest neighbors. Specifically, the method begins by first calculating the MI using entropy<sup>15</sup> as

$$I(X;Y) = H(X) + H(Y) - H(X,Y), \quad (\text{A3})$$

where  $H$  is the Shannon entropy. Next, an approximation of  $H(X)$  with digamma functions is done, but the probability density of  $X$  and  $Y$  still needs to be estimated. To do this, adaptive partitions using the  $k$ -nearest neighbor are formed. Specifically Kraskov et al. develop two different partitioning methods with similar results. The first method uses the maximum Chebyshev distance to the  $k = 1$  nearest neighbor  $j$  to form square bins as shown in Fig. 19-a, and the second method in Fig. 19-b uses rectangular partitions using the horizontal and vertical distances to the  $k = 1$  nearest neighbor  $j$ . To con-

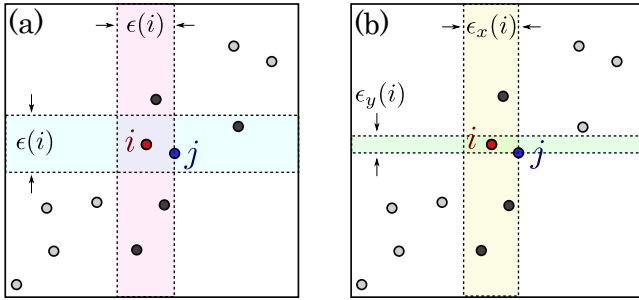


FIG. 19. Example showing two different partition methods for Mutual Information estimation using  $k = 1$  nearest neighbor adaptive partitioning.

tinue with the example shown in Fig. 19, the density probability is estimated using the strips formed from these bins. To highlight the difference, Fig. 19-a shows a horizontal strip of width  $\epsilon(i)$  encapsulating  $n_x(i) = 2$  points (strip does not include the point  $i$ ), while in Fig. 19-b only  $n_x(i) = 1$  point is enclosed. Using these probability density approximations and the digamma function  $\psi$ , MI between  $X$  and  $Y$  can be estimated. Using the partitioning method shown in Fig. 19-a the MI is estimated as

$$I^{(1)}(X;Y) = \psi(k) - (\psi(n_x + 1) + \psi(n_y + 1) + \psi(N)). \quad (\text{A4})$$

Using the partitioning method shown in Fig. 19-b the MI is estimated as

$$I^{(2)}(X;Y) = \psi(k) - 1/k - [\psi(n_x) + \psi(n_y)] + \psi(N). \quad (\text{A5})$$

For the results shown in Section IV, we use the  $k = 3$  nearest neighbor to generate the partitions.

## 5. Dynamic System Models

### a. Lorenz System

The Lorenz system used is defined as

$$\frac{dx}{dt} = \sigma(y - x), \quad \frac{dy}{dt} = x(\rho - z) - y, \quad \frac{dz}{dt} = xy - \beta z. \quad (\text{A6})$$

The Lorenz system had a sampling rate of 100 Hz with parameters  $\sigma = 10.0$ ,  $\beta = 8.0/3.0$ , and  $\rho = 95$ . This system was solved for 100 seconds and the last 24 seconds were used.

### b. Rössler System

The Rössler system used was defined as

$$\frac{dx}{dt} = -y - z, \quad \frac{dy}{dt} = x + ay, \quad \frac{dz}{dt} = b + z(x - c), \quad (\text{A7})$$

with parameters of  $a = 0.1$ ,  $b = 0.1$ ,  $c = 14$ , which was solved over 400 seconds with a sampling rate of 10 Hz. Only the last 1500 data points of the  $x$ -solution were used in the analysis.

### c. Bi-Directional Coupled Rössler System

The Bi-directional Rössler system is defined as

$$\begin{aligned} \frac{dx_1}{dt} &= -w_1 y_1 - z_1 + k(x_2 - x_1), \\ \frac{dy_1}{dt} &= w_1 x_1 + 0.165 y_1, \\ \frac{dz_1}{dt} &= 0.2 + z_1(x_1 - 10), \\ \frac{dx_2}{dt} &= -w_2 y_2 - z_2 + k(x_1 - x_2), \\ \frac{dy_2}{dt} &= w_2 x_2 + 0.165 y_2, \\ \frac{dz_2}{dt} &= 0.2 + z_2(x_2 - 10), \end{aligned} \quad (\text{A8})$$

with  $w_1 = 0.99$ ,  $w_2 = 0.95$ , and  $k = 0.05$ . This was solved for 4000 seconds with a sampling rate of 10 Hz. Only the last 400 seconds of the  $x$ -solution were used in the analysis.

### d. Mackey-Glass Delayed Differential Equation

The Mackey-Glass Delayed Differential Equation is defined as

$$\dot{x}(t) = -\gamma x(t) + \beta \frac{x(t - \tau)}{1 + x(t - \tau)^n} \quad (\text{A9})$$

with  $\tau = 2$ ,  $\beta = 2$ ,  $\gamma = 1$ , and  $n = 9.65$ . This was solved for 400 seconds with a sampling rate of 100 Hz. The solution was then downsampled to 5 Hz and only the last 1500 terms of the  $x$ -solution were used in the analysis.

**e. Periodic Sinusoidal Function**

The sinusoidal function is defined as

$$x(t) = \sin(2\pi t) \quad (\text{A10})$$

This was solved for 10 seconds with a sampling rate of 50 Hz.

**f. EEG Data**

The EEG signal was taken from andrzejak et al.<sup>2</sup>. Specifically, the first 2000 data points from the EEG data of a healthy patient from set A, file Z-093 was used.

**g. ECG Data**

The Electrocardiogram (ECG) data was taken from SciPy's misc.electrocardiogram data set. This ECG data was originally provided by the MIT-BIH Arrhythmia Database<sup>35</sup>. We used data points 3000 to 4500 during normal sinus rhythm.

**h. Logistic Map**

The logistic map was generated as

$$x_{n+1} = rx_n(1 - x_n), \quad (\text{A11})$$

with  $x_0 = 0.5$  and  $r = 3.95$ . Equation A11 was solved for the first 500 data points.

**i. Hénon Map**

The Hénon map was solved as

$$\begin{aligned} x_{n+1} &= 1 - ax_n^2 + y_n, \\ y_{n+1} &= bx_n, \end{aligned} \quad (\text{A12})$$

where  $b = 0.3$ ,  $x_0 = 0.1$ ,  $y_0 = 0.3$ , and  $a = 1.4$ . This system was solved for the first 500 data points of the x-solution.

**6. Tabulated PE parameters**

System	Mutual Information				Suggested Delay $\tau$	Ref.
	Equal-sized Partitions	Kraskov et al. Method 1	Kraskov et al. Method 2	Adaptive Partitions		
White Noise	<b>1</b>	3	3	<b>1</b>	1	44
Lorenz	13	<b>9</b>	<b>9</b>	<b>9</b>	10	44
Rosler	14	13	<b>11</b>	<b>9</b>	9	50
Bi-directional Rosler	<b>16</b>	<b>14</b>	<b>14</b>	<b>15</b>	15	44
Mackey-Glass	<b>7</b>	<b>8</b>	<b>7</b>	<b>7</b>	1 to 700	44
Sine Wave	4	<b>17</b>	<b>13</b>	1	15	50
Logistic Map	<b>5</b>	8	11	<b>5</b>	1 to 5	44
Henon Map	12	15	13	8	1 to 5	44
ECG	22	16	9	8	1 to 4	44
EEG	6	5	5	5	1 to 3	44

TABLE I. A comparison between the calculated and suggested values for the delay parameter  $\tau$  for multiple MI approximation methods. The cells in bold highlight the methods that yielded the closest match to the suggested delay. The equal-sized partition method is described in Section A 4 a, Kraskov et al. methods 1 and 2 in Section A 4 c, and the adaptive partitioning approach in Section A 4 b.

Category	System	Traditional Methods		Modified/Proposed Methods			Suggested Delay ( $\tau$ )	Ref.
		MI using AP	Spearman's AC	Freq. App.	MPE	PAMI ( $4 \leq n \leq 6$ )		
Noise	White Noise	1	<b>1</b>	<b>1</b>	<b>1</b>	<b>1</b>	1	44
Chaotic Differential Equation	Lorenz	<b>9</b>	15	6	17	<b>5 to 9</b>	10	44
	Rosler	<b>9</b>	12	<b>7</b>	19	<b>6 to 10</b>	9	50
	Bi-directional Rosler	<b>15</b>	<b>12</b>	7	20	6 to 10	15	44
	Mackey-Glass	<b>7</b>	<b>5</b>	<b>3</b>	<b>8</b>	<b>2 to 4</b>	1 to 700	44
Periodic	Sine Wave	1	<b>10</b>	<b>21</b>	<b>16</b>	5 to 8	15	50
Nonlinear Difference Eq.	Logistic Map	<b>5</b>	<b>1</b>	<b>1</b>	<b>1</b>	<b>1</b>	1 to 5	44
	Henon Map	8	<b>1</b>	<b>1</b>	<b>1</b>	<b>1</b>	1 to 5	44
Medical Data	ECG	8	21	<b>2</b>	13	<b>1 to 2</b>	1 to 4	44
	EEG	<b>5</b>	<b>4</b>	<b>1</b>	<b>4</b>	<b>2 to 4</b>	1 to 3	44

TABLE II. A comparison between the calculated and suggested values for the delay parameter  $\tau$ . The cells in bold show the methods that yielded the closest match to the suggested delay. The following conditions or abbreviations were used in the table: the range under PAMI results is from using the range ( $4 < n < 6$ ), AP under MI is an abbreviation for adaptive partitioning, and AC is an abbreviation for autocorrelation.

Category	System	Traditional Methods		Modified Method	Suggested Dim. (n)	Ref.
		FNN	SSA	MPE		
Noise	White Noise	<b>4</b>	23	<b>5</b>	3 to 7	44
Chaotic Differential Equation	Lorenz	3	4	<b>5</b>	5 to 7	44
	Rosler	4	4	4	6	50
	Bi-directional Rosler	4	4	4	6 to 7	44
	Mackey-Glass	<b>4</b>	<b>6</b>	<b>4</b>	4 to 8	44
Periodic	Sine Wave	<b>4</b>	2	3	4	50
Nonlinear Difference Equation	Logistic Map	<b>4</b>	<b>3</b>	<b>5</b>	2 to 16	44
	Henon Map	<b>4</b>	2	<b>5</b>	3 to 10	44
Medical Data	ECG	<b>7</b>	8	<b>5</b>	3 to 7	44
	EEG	<b>5</b>	11	<b>6</b>	3 to 7	44

TABLE III. A comparison between the calculated and suggested values for the embedding dimension  $n$ . The cells in bold show the methods that yielded the closest match to the suggested dimension.